AMERICAN SOCIETY FOR MICROBIOLOGY | mBio®

RESEARCH ARTICLE
Host-Microbe Biology

Neuroinflammatory Changes in Relation to Cerebrospinal Fluid Viral Load in Simian Immunodeficiency Virus Encephalitis

Dima A. Hammoud,[a] Sanhita Sinharay,[a] Swati Shah,[a] William Schreiber-Stainthorp,[a] Dragan Maric,[b] Siva Muthusamy,[a] Dianne E. Lee,[a] Cheri A. Lee,[e] Falguni Basuli,[c] William C. Reid,[a] Paul Wakim,[d] Kenta Matsuda,[e] Vanessa Hirsch,[e] Avindra Nath,[f] Michele Di Mascio[g]

[a]Center for Infectious Disease Imaging, Radiology and Imaging Sciences, Clinical Center, National Institutes of Health, Bethesda, Maryland, USA
[b]Division of Intramural Research, National Institute of Neurological Disorders and Stroke, National Institutes of Health, Bethesda, Maryland, USA
[c]Imaging Probe Development Center, National Heart, Lung, and Blood Institute, National Institutes of Health, Rockville, Maryland, USA
[d]Biostatistics and Clinical Epidemiology Service, Clinical Center, National Institutes of Health, Bethesda, Maryland, USA
[e]Laboratory of Molecular Microbiology, National Institute of Allergy and Infectious Diseases, National Institutes of Health, Bethesda, Maryland, USA
[f]Section of Infections of the Nervous System, National Institute of Neurological Disorders and Stroke, National Institutes of Health, Bethesda, Maryland, USA
[g]AIDS Imaging Research Section, Division of Clinical Research, National Institute of Allergy and Infectious Diseases, National Institutes of Health, Rockville, Maryland, USA

ABSTRACT The exact cause of neurocognitive dysfunction in HIV-positive patients despite successful control of the infection in the periphery is not completely understood. One suggested mechanism is a vicious cycle of microglial activation and release of proinflammatory chemokines/cytokines that eventually leads to neuronal loss and dysfunction. However, the exact role of microglial activation in the earliest stages of the infection with high cerebrospinal fluid (CSF) viral loads (VL) is unclear. In this study, we imaged the translocator protein (TSPO), a mitochondrial membrane receptor known to be upregulated in activated microglia and macrophages, in rhesus macaques before and multiple times after inoculation with a neurotropic simian immunodeficiency virus (SIV) strain (SIVsm804E), using 18F-DPA714 positron emission tomography (PET). The whole-brain standardized uptake values of TSPO at equilibrium reflecting total binding (SUV_T) and binding potentials (BP_{ND}) were calculated and correlated with CSF and serum markers of disease, and a corresponding postmortem immunostaining analysis was also performed. SUV_T was found to be inversely correlated with both CSF VL and monocyte chemoattractant protein 1 (MCP-1) levels. In SIV-infected macaques with very high CSF VL at necropsy ($>10^6$ copies/ml), we found decreased TSPO binding by PET, and this was supported by immunostaining which showed glial and neuronal apoptosis rather than microglial activation. On the other hand, with only moderately elevated CSF VL ($\sim10^4$ copies/ml), we found increased TSPO binding as well as focal and diffuse microglial activation on immunostaining. Our results in the SIV-infected macaque model provide insights into the relationship between HIV neuropathology and CSF VL at various stages of the disease.

IMPORTANCE Neurological and cognitive problems are a common complication of HIV infection and are prevalent even in treated individuals. Although the molecular processes underlying brain involvement with HIV are not completely understood, inflammation is suspected to play a significant role. Our work presents an *in vivo* assessment of neuroinflammation in an animal model of HIV, the simian immunodeficiency virus (SIV)-infected rhesus macaque. Using positron emission tomography (PET) imaging, we identified changes in brain inflammation after inoculation with SIV over time. Interestingly, we found decreased binding of the PET ligand in the presence of very high cerebrospinal fluid (CSF) viral loads. These findings were supported by immunostaining which showed marked glial loss instead of inflammation. This study provides insight into glial and neuronal changes associated with very

Citation Hammoud DA, Sinharay S, Shah S, Schreiber-Stainthorp W, Maric D, Muthusamy S, Lee DE, Lee CA, Basuli F, Reid WC, Wakim P, Matsuda K, Hirsch V, Nath A, Di Mascio M. 2019. Neuroinflammatory changes in relation to cerebrospinal fluid viral load in simian immunodeficiency virus encephalitis. mBio 10:e00970-19. https://doi.org/10.1128/mBio.00970-19.

Invited Editor Shilpa Buch, UNMC

Editor Vinayaka R. Prasad, Albert Einstein College of Medicine

Address correspondence to Dima A. Hammoud, hammoudd@cc.nih.gov.

Received 17 April 2019
Accepted 29 April 2019
Published 28 May 2019

high CSF viral load and could reflect similar changes occurring in HIV-infected patients.

KEYWORDS DPA714, SIV encephalitis, neuroinflammation, positron emission tomography, rhesus macaques, translocator protein

A major question in HIV pathophysiology is the effect of the virus on the brain in the course of infection, before and after the initiation of antiretroviral therapy (ART). This question has not yet been fully answered in humans due to the paucity of pathological specimens available from HIV patients. One hypothesized cause of neuropathology in HIV is a constant neuroinflammatory burden resulting in a vicious cycle of microglial activation, release of chemokines/cytokines, and neuronal loss/dysfunction (1–6). The exact contribution of neuroinflammation to neuronal damage in various stages of infection before cerebrospinal fluid (CSF) viral load (VL) reaches a set point, mainly in the earliest stages of the infection with high CSF VL, remains unclear.

Neuroinflammation can be imaged *in vivo* using positron emission tomography (PET) ligands targeted against the translocator protein (TSPO), an outer mitochondrial membrane receptor known to be upregulated under inflammatory conditions (6). In this study, we used an animal model of HIV, the simian immunodeficiency virus (SIV)-infected monkey, to better characterize brain pathological changes associated with high CSF VL such as those seen in some patients during the early stages of HIV infection (7). Toward this goal, we performed longitudinal PET imaging of the monkeys before and after SIV inoculation using 18F-DPA714, a commonly used TSPO ligand (8–10). The animals were inoculated with SIVsm804E, a neurovirulent SIV strain capable of establishing early central nervous system (CNS) infection and causing neuropathology with very high CSF VLs in almost 80% of susceptible animals (based on Trim5α and major histocompatibility complex [MHC] genotypes) (11). We correlated our PET findings with CSF cytokine levels and $CD4^+$ T-cell counts as well as CSF and plasma VL. We performed an RNAscope assay to detect the presence of the virus in the brains of infected animals and multiplex immunofluorescence (MIF) staining of microglial, astrocytic, and neuronal cell populations postmortem in both SIV-infected and control animals.

RESULTS

Course of disease. A detailed description of the animal characteristics and dates of various procedures for all the animals is included in Table S1 in the supplemental material. Graphs showing the relationship between CSF VL, plasma VL, and select CSF cytokines/chemokines are also included in Fig. S2 for all animals.

Briefly, two out of five animals (SIV#1 and -2) developed symptoms within 5 to 9 weeks from inoculation with CSF VL levels of $>10^6$. Both animals were treated with a combination of tenofovir (PMPA), emtricitabine (FTC), and raltegravir. One animal (SIV#2), however, did not respond to treatment and succumbed to the disease 11 weeks after inoculation. SIV#1 responded to nonsuppressive treatment with resolution of neurological symptoms and decreased plasma and CSF VL levels. Treatment was eventually stopped to allow progression to terminal disease, and imaging followed by necropsy was performed 20 weeks later (CSF VL, $\sim10^6$ copies/ml).

SIV#3 did not develop symptoms until 93 weeks after inoculation. The animal was treated and responded to nonsuppressive treatment, which was eventually interrupted 108 weeks postinoculation to allow progression to terminal disease. The animal was euthanized approximately 15 weeks after treatment interruption (124 weeks postinoculation; CSF VL, $\sim10^4$ copies/ml). The course of disease for SIV#4 was complicated by hydrocephalus developing around 80 weeks after inoculation, which we believe was caused by an opportunistic CNS infection. In order to avoid the confounding effects of such an infectious process on imaging, only 18F-DPA714 scans obtained before the development of hydrocephalus are included in the imaging analysis. Brain immunostaining and RNAscope data for this animal were also excluded for the same reasons.

SIV#5 progressed 33 weeks postincoculation but did not respond to treatment. Only the early follow-up scan on this animal is included in the analysis due to technical problems associated with its preeuthanasia scan. The animal CSF VL at necropsy was $\sim 10^6$ copies/ml.

18F-DPA714 PET imaging. An example of the time activity curves from multiple regions of one of the animals (SIV#1) is shown in Fig. 1A. For one of the animals (SIV#4), proper displacement with PK11195 could not be achieved for unclear reasons; hence, analysis was based on total standardized uptake value (SUV_T) for this subject (animal excluded from the binding potential [BP_{ND}] analysis).

In the 4 animals that had successful displacement, we noticed that the various evaluated brain regions had very similar nonspecific binding (Fig. 1A). Nonspecific binding in each animal was also very comparable across the various studies despite changes in total binding. An example of comparable nonspecific binding can be seen in Fig. 1B with similar SUV values seen after displacement in two studies acquired at two time points from the same animal.

Comparing the preinoculation and last imaging sessions, 4 out of 5 animals showed lower BP_{ND} and/or SUV_T than their preinoculation baselines. An example of one of the animals, SIV#1, is shown in Fig. 1C. One out of 5 animals (SIV#3) showed the opposite, with higher binding at the last time point compared to preinoculation scans (Fig. 1D).

Immunofluorescence. Iba1 staining (used to delineate microglia and peripherally derived macrophages in the brain [12]) was decreased in 3 animals with high CSF VL at necropsy (SIV#1, -2, and -5; CSF VL, $\sim 10^6$ copies/ml) compared to controls (Fig. 2A and B and Fig. 3) while it was increased in SIV#3, the one animal which had lower CSF VL at necropsy ($\sim 10^4$ copies/ml) and increased TSPO binding on PET prior to necropsy (Fig. 2C and Fig. 3). In this animal, the microglia appeared enlarged/amoeboid in shape with thickened ramifications.

We also found increased CC3/poly(ADP-ribose) polymerase (PARP) staining, reflecting apoptotic cells (13), in all infected animals (Fig. 2B and C and Fig. 3). In general, CC3/PARP in the infected animals colocalized with neurons (NeuN positive) but also with microglia/macrophages (Iba1 positive) and astrocytes (S100 positive) (Fig. 4). NeuN staining was slightly decreased in two animals compared to controls and slightly increased in one (SIV#2). This is probably due to the fact that SIV#2 was euthanized shortly after inoculation. We also assessed NeuN in the striatal area, but not in the cortex, which could have affected our neuronal count results.

SIV#1, -3, and -5 showed microglial nodules with increased Iba1 and CC3/PARP and decreased S100 staining compared to surrounding tissues (Fig. S3). The nodules were mainly seen in the white matter, but a few were also seen in deep gray matter structures. SIV#2 did not show microglial nodules, probably due to the short length of infection prior to necropsy ($\sim$11 weeks postinoculation).

RNAscope assay. In SIV#1, -3, and -5, SIV RNA was detected in the subcortical white matter as well as in the striatum, mainly in association with microglial nodules but also within the surrounding parenchyma. SIV-specific RNA was detected in the brain of SIV#2 in a more diffuse distribution despite the absence of microglial nodules (Fig. 5).

Cytokine/chemokine measurements in the CSF. Based on the previously available literature about the changes in cytokine expression during HIV-1 infection and the availability of nonhuman primate-specific antibodies, we chose a panel of 23 cytokines to test (14–16). The levels of granulocyte-macrophage colony-stimulating factor (GM-CSF), IL-17a, IL-4, IL-5, IL-13, MIP-1β, and IL-1β were undetectable in the CSF of our animals at baseline and follow-up evaluations. We, however, found increased concentrations of monocyte chemoattractant protein 1 (MCP-1), tumor necrosis factor alpha (TNF-α), gamma interferon (IFN-γ), IL-1Ra, IL-2, IL-6, IL-8, IL-10, IL-12, and IL-18 in the CSF after inoculation compared to preinoculation values in most animals, which corresponded to increased CSF VL while there was little to no change in the levels of the remaining cytokines/chemokines between baseline and follow-ups. The changes in the cytokine levels varied depending on the treatment status. Depictions of CSF/plasma

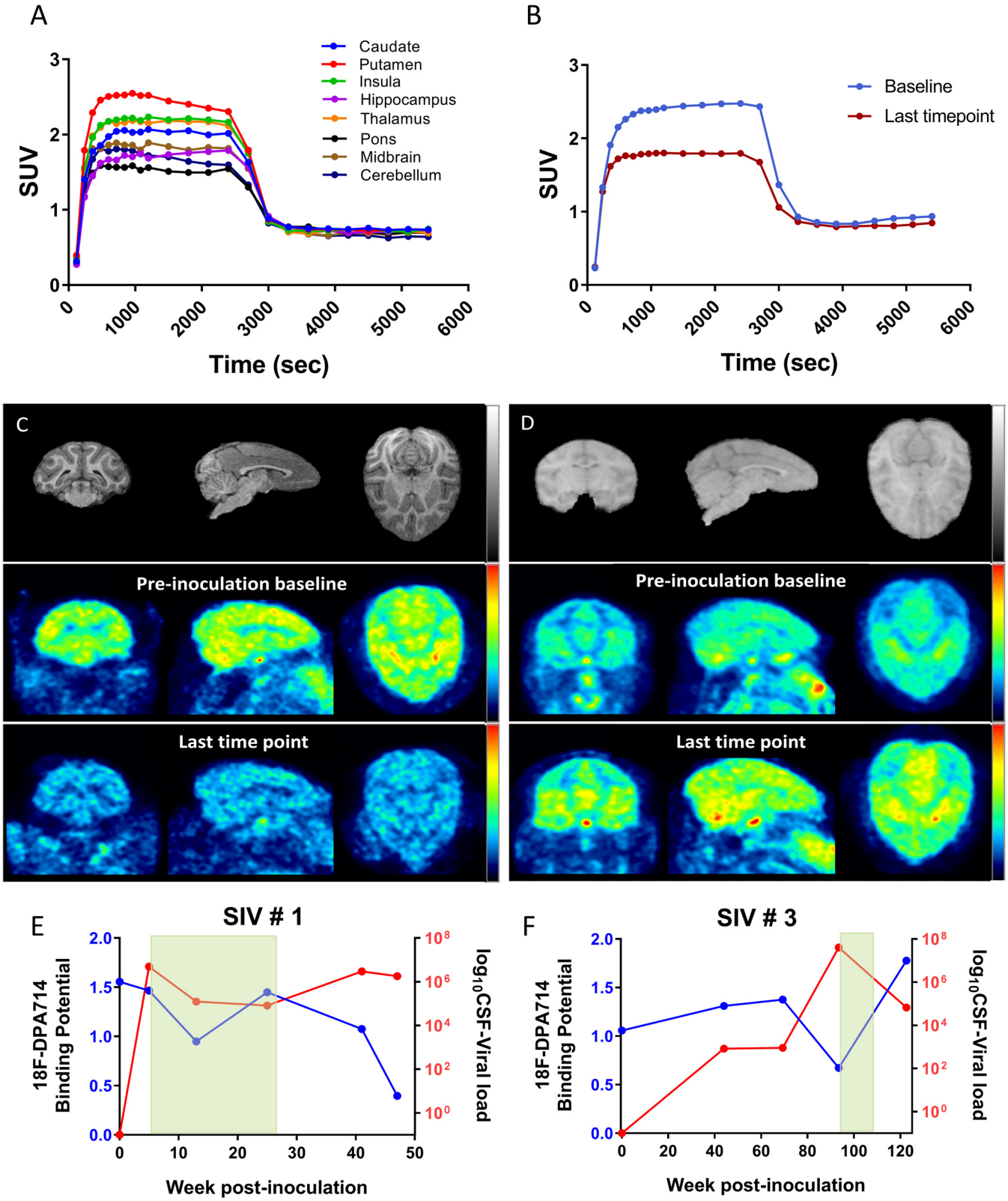

FIG 1 (A) Time-activity curve (TAC) of 18F-DPA714 PET scan in SUV#1 shows different levels of total binding in different regions (SUV at equilibrium) with stable nonspecific binding (equilibrium after displacement). (B) TACs of the putaminal VOI in SIV#1 show decreased total binding at the last time point prior to necropsy (red line) compared to preinoculation (blue line) with relatively stable nonspecific binding. (C and D) SIV#1 (C) and SIV#3 (D) preinoculation and postinoculation, prenecropsy 18F-DPA714 PET scans (reflecting SUV_T). While SIV#1 showed decreased uptake, SIV#3 showed increased uptake at the last time point. (E and F) Corresponding changes of CSF VL and BP_{ND} values for the same two animals over the course of their disease (green boxes reflect treatment [ART] courses).

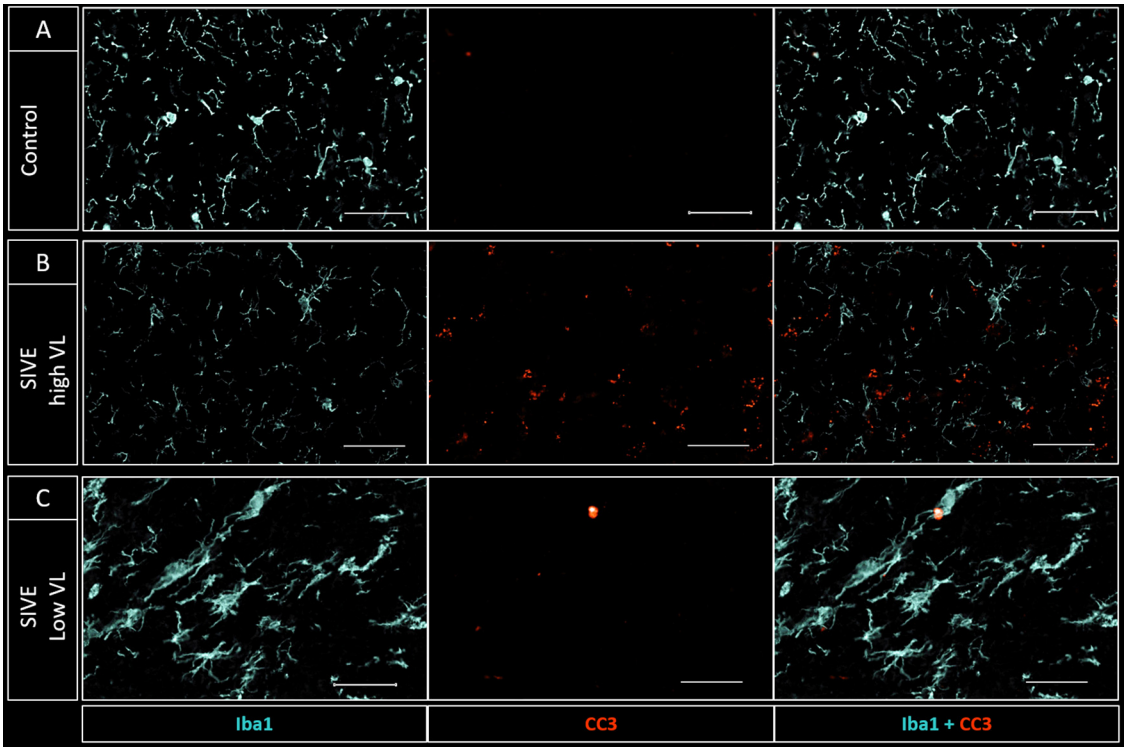

FIG 2 Iba1 (light blue) and CC3/PARP (red) staining of white matter tracts in a control (A) and two infected animals (B and C). (B) SIV#1 (CSF VL of ~10^6 at necropsy) shows decreased Iba1 and increased CC3/PARP staining, suggesting microglial loss/dysfunction and increased apoptosis compared to control. (C) SIV#3 (CSF VL of ~10^4) shows increased Iba1 staining with amoeboid-shaped cell bodies and truncated processes consistent with microglial activation. There is lower CC3/PARP staining than with SIV#1 but higher than with control (bar, 100 μm).

VL and their relationship to CSF cytokines/chemokines and treatment (if applicable) are included for all animals in Fig. S2. In the two animals that responded to treatment (SIV#1 and SIV#3), CSF cytokine levels decreased concomitantly with decreased CSF and plasma viral loads, often reaching baseline preinfection levels, even though we did not achieve complete suppression of the infection in the brain. Those cytokines, however, later rebounded after interruption of therapy (the green-highlighted areas in the graphs in Fig. S2 reflect the duration of treatment), especially MCP-1. The two animals who did not respond to treatment, however, were euthanized before the cytokine levels in the CSF started to normalize. There were no appreciable decreases in the CSF or plasma VL in either of those two animals prior to euthanasia.

Statistical analyses. A repeated-measures mixed-model approach ($n = 18$ scans obtained on 5 animals) indicated that CSF VL was a statistically significant predictor of whole-brain (WB) SUV_T with a negative regression coefficient ($P = 0.036$, effect size based on Cohen's $f^2 = 0.62$ [17]). Among the cytokines, only CSF MCP-1 showed a statistically significant relationship with whole-brain SUV_T, which was also negative ($P = 0.044$, $f^2 = 0.33$).

For the BP_{ND} values, we found a negative relationship between CSF VL and whole-brain BP_{ND} values; however, this did not reach significance ($P = 0.064$, $f^2 = 0.18$). In the latter analysis, only 4 animals (15 observations) were used since one of the animals did not show adequate displacement (SIV#4).

DISCUSSION

Our main goal in this study was to identify dynamic TSPO expression changes, reflecting the neuroinflammatory burden, at various CSF VL values in the setting of SIV encephalitis (SIVE), using a combination of longitudinal PET imaging and multiplex immunofluorescence. We found evidence of microglial loss/dysfunction, manifested as

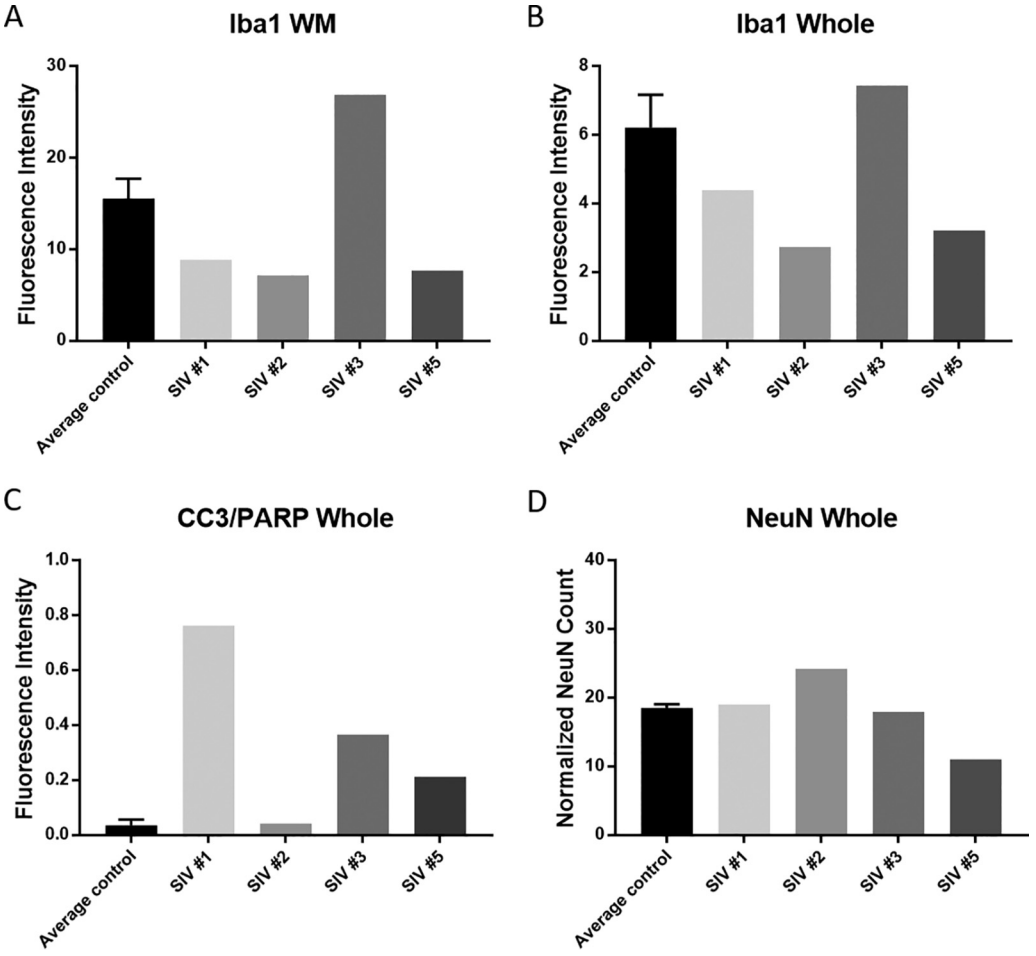

FIG 3 Quantitative assessment of Iba1 (microglia/macrophages) (A and B), CC3/PARP (apoptosis) (C), and NeuN (neuron) (D) staining in SIV-infected animals compared to average control values (WM, white matter; whole, striatum and white matter). Error bars represent standard deviation values derived from two control animals.

decreased 18F-DPA714 uptake/binding on PET, rather than microglial activation, in 4 out of 5 SIV-infected monkeys with very high CSF VL (Fig. 1). Histopathology confirmed our findings, showing decreased Iba1 staining and increased CC3/PARP staining in animals with very high CSF VL ($>10^6$ copies/ml) compared to two uninfected animals (Fig. 2 and 3). We confirmed colocalization of apoptosis markers with Iba1, S100, and NeuN staining, suggesting macrophage and glial death/dysfunction but, more importantly, neuronal death (Fig. 4). Based on our observations in the SIV-infected monkeys, we believe a similar process could be occurring in HIV^+ patients with high CSF VL, with possible associated neuronal loss occurring in the setting of viral replication. This neuronal loss could potentially account for a certain degree of irreversible CNS damage in HIV.

One of our infected animals with only moderately elevated CSF VL at necropsy ($\sim 10^4$ copies/ml), on the other hand, was found to have increased 18F-DPA714 binding at the last point (prenecropsy scan) compared to baseline (preinoculation), which corresponded to microglial activation on immunohistochemistry (IHC). This animal is thus more reflective of chronically infected HIV-positive (HIV^+) subjects who have reached their viral set point. Since our monkey antiretroviral treatment regimen was not completely suppressive, however, we cannot assume that our findings also reflect changes in optimally treated patients. Using a repeated-measures mixed-effect model, we found a negative correlation between 18F-DPA714 SUV_T values and CSF VL levels, with higher CSF VL values corresponding to lower binding, suggesting microglial

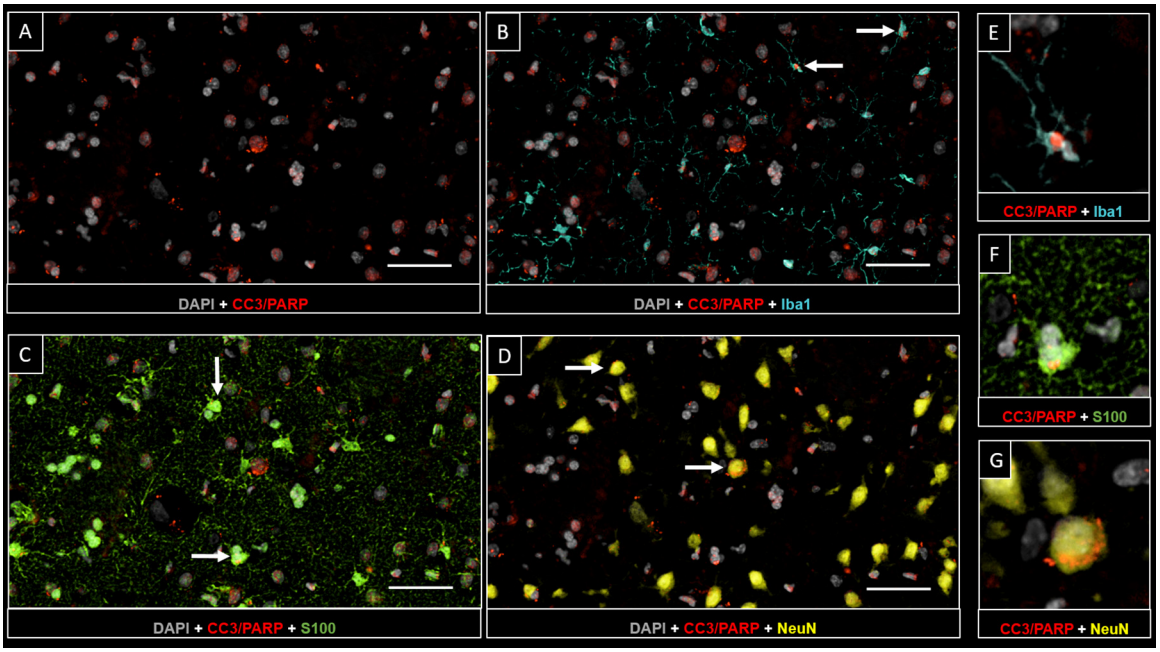

FIG 4 (A to D) DAPI (gray) and CC3/PARP (red) (A); DAPI (gray), CC3/PARP (red), and Iba1 (light blue) (B); DAPI (gray), CC3/PARP (red), and S100 (green) (C); and DAPI (gray), CC3/PARP (red), and NeuN (yellow) (D) staining obtained in SIV#1 (bar, 50 μm). (E to G) In animals with very high CSF VL at necropsy ($>10^6$), apoptotic markers colocalized with microglial (E), astrocytic (F), and neuronal (G) markers.

loss/dysfunction. We believe that a larger sample number would further confirm those findings and might detect correlations with other CSF cytokine levels. We also found a negative correlation between 18F-DPA714 SUV_T and CSF levels of MCP-1. Of note, even though CSF cytokines changed in parallel with CSF and plasma VL values, after treatment initiation and treatment interruption, they probably do not accurately reflect parenchymal microglial activation patterns.

So what causes microglial dysfunction/loss in the setting of very high CSF VL? Microglia and macrophages are known to be infected by HIV and SIV (18–20) and have been proposed to act as reservoirs for the virus (21, 22). Recently, however, it has been proposed that acute infection of human microglia and macrophages instead results in

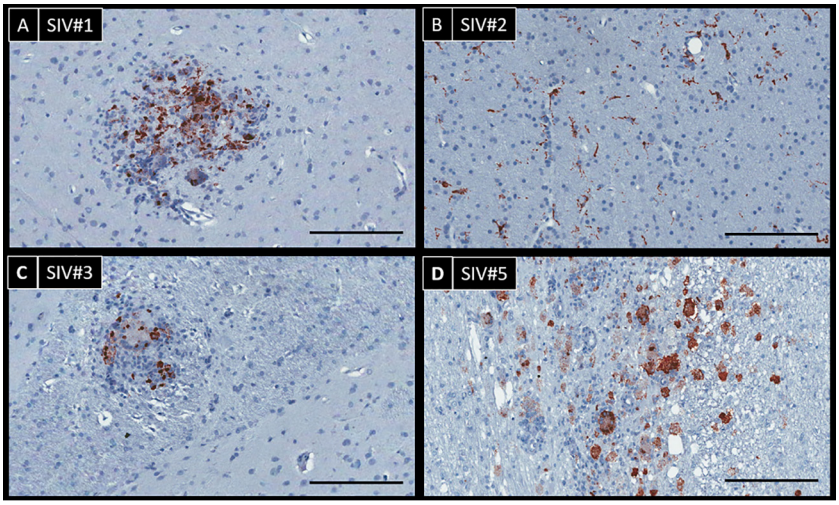

FIG 5 SIV-specific staining (brown staining indicates the presence of viral RNA) of brain sections of rhesus macaques with SIVE showing characteristic glial nodules containing multinucleated giant cells in SIV#1 (A), SIV#3 (C), and SIV#5 (D). In SIV#2 (B), there were no microglial nodules and SIV-specific staining was seen in a more diffuse distribution throughout the parenchyma.

apoptosis, with only a small population of those cells eventually surviving the infection and silencing viral replication, thus becoming viral reservoirs (21). Another study showed evidence of a senescence-like phenotype in cultures of human fetal microglia after exposure to HIV (23). Direct infection of microglia/macrophages is thus perhaps responsible for the apoptotic changes and dysfunction/lack of activation in the presence of overwhelmingly high CSF VLs. This is further confirmed by the presence of SIV RNA in the brain tissues of our animals and by its colocalization with microglial nodules (11, 24, 25). Interestingly, in one of the animals that died in the early stages of the disease (SIV#2), SIV RNA staining seemed similar in shape to microglial cells (Fig. 5). Without costaining with glial markers, however, this observation cannot be confirmed. With decreased CSF VL values, on the other hand, a neuroinflammatory pattern is seen. This probably reflects activation of residual microglia as well as further recruitment of peripherally derived macrophages to the brain.

Our techniques, namely PET imaging and multiplex immunofluorescent staining, are complementary: while PET allows the depiction of *in vivo* longitudinal changes in TSPO expression in the brain, reflecting microglial activation or dysfunction, postmortem staining confirms those findings, albeit at just one time point. Our PET ligand, 18F-DPA714, is one of the most commonly used second-generation TSPO ligands and has been useful in the study of other animal models of neuroinflammation, including encephalitis (26), and other preclinical neurodegenerative disease models. Previous attempts to image microglial activation *in vivo* in treated HIV^+ patients using 11C-PK11195 PET yielded inconsistent results, probably due to the heterogeneity of patient populations and limitations of the radiotracer (8, 9, 26, 27). More recent attempts to image TSPO using 11C-DPA713 (28) and 11C-PBR28 (29) showed evidence of persistent neuroinflammation despite treatment. Although we did not achieve suppression of CSF VL with our treatment regimen, increased TSPO binding in SIV#1 and -3 when CSF VL levels decreased under the effect of treatment (Fig. 1E and F) could possibly be similar to human findings of persistent neuroinflammation despite treatment. One interesting observation was that we did not detect sex-specific differences in disease progression or neuroinflammatory changes; however, we believe our sample number might be too small to draw a definite conclusion.

Our study is limited by small sample number and by slow progression of disease in two animals. Both male and female monkeys were included, as the Q/Q genotype we screened for is relatively rare. Due to the logistical limitations associated with the infectious nature of the SIV model, we were not able to perform arterial blood sampling and therefore could not perform compartmental analysis of our PET scans using a plasma input function. On the other hand, no suitable reference region is available for TSPO binding in this model, owing to the diffuse neuropathology of SIV encephalitis (SIVE). To overcome those issues, we resorted to a bolus/infusion (B/I) approach for imaging, which is considered generally more accurate than bolus injection alone since true equilibrium rather than a transient equilibrium can be reached (30). The B/I model also allowed us to perform displacement with cold PK11195, an antagonist of TSPO, in order to displace DPA714 and measure nonspecific binding. We employed the commonly used PK11195 dose for displacement, which we believe successfully achieved maximum displacement, as supported by very comparable nonspecific binding established in all evaluated regions (Fig. 1A). In addition, the nonspecific binding in the whole brain and various regions was generally constant across the longitudinal scans (Fig. 1B) despite a change in total binding values. B/I methods are also much less affected by changes in plasma clearance than bolus-only methods (30).

In conclusion, using a combination of PET imaging and immunostaining, we found evidence of glial (microglia and astrocytes) and neuronal damage in association with very high CSF VL in SIV-infected monkeys, which we believe could simulate brain pathology associated with high CSF VL values in HIV infection. Whether this could explain, at least partially, the irreversible component of neuronal injury in HIV still needs to be evaluated in a larger sample number and in human studies.

MATERIALS AND METHODS

Animals. All experiments were approved by the Institutional Animal Care and Use Committee of the National Institute of Allergy and Infectious Diseases (NIAID), National Institutes of Health. A total of 50 rhesus macaques were screened for Trim5α genotype, and 5 animals (SIV#1, -2, -3, -4, and -5) with Q/Q genotype were chosen for this study as they are known to be susceptible to development of SIV encephalitis (SIVE) (11, 31, 32). The selected animals included females ($n = 3$) and males ($n = 2$) (age range, 33 to 58 months), which was necessary given the rarity of the Q/Q genotype. SIV#1/SIV#2 and SIV#3/SIV#4 were socially housed in pairs (same gender) prior to infection, separated until the infection was confirmed, and then paired again. When one of the animals had to be euthanized, however, the other animal was not paired with any other animals and was singly housed until euthanasia. SIV#5 was singly housed. All animals underwent PET and magnetic resonance imaging (MRI) at preinoculation baseline and multiple time points after intravenous inoculation with SIVsm804E. Imaging sessions were based on progression of disease and response to treatment, if applicable. Throughout the study, we carefully monitored the animals for neurologic symptoms (tremor, balance issues, head tilt, difficulty perching, and decreased motor coordination). Plasma and CSF VL as well as $CD4^+$ T-cell counts and CSF cytokines were measured throughout the disease course. When the animals were treated, the ART regimen consisted of daily subcutaneous injections of tenofovir (PMPA; 20 mg/kg of body weight) and emtricitabine (FTC; 30 mg/kg) with raltegravir (20 mg/kg) mixed with food twice per day.

For both the MRI and PET studies, the animals were anesthetized using a combination of ketamine (~0.1 ml/kg) and propofol (0.2 mg/kg/min). The concentrations of various anesthetics as well as the timing of administration with respect to imaging were kept constant across the studies to minimize the potential effects of anesthesia on TSPO binding on the uptake of second-generation TSPO ligands, including 18F-DPA714 (33, 34). During imaging, the animals were carefully monitored for changes in body temperature, oxygen saturation, and heart and respiratory rates.

18F-DPA714 PET imaging and analysis. 18F-DPA714 was synthesized as previously reported (35). PET scans were performed on a high-resolution research tomograph (CPS/CTI-HRRT; Siemens) scanner (spatial resolution, 2.4 by 2.4 by 2.8 mm). After a transmission scan was obtained for calculation of attenuation correction maps, 18F-DPA714 was administered intravenously using a bolus/infusion approach (mean injected dose = 184.36 ± 18.08 MBq [4.98 ± 0.48 mCi], radiochemical purity of >99%, $K_{bol} = 50$; 50% of the dose administered as bolus with the rest infused over 90 min). Exactly 45 min after starting the 18F-DPA714 injection, cold (nonradioactive) PK11195 (3 mg/kg), a TSPO antagonist, was injected either as a bolus injection followed by a quick saline flush or as a bolus/infusion approach ($K_{bol} = 50$). Imaging was continued for another 45 min (total scanning time = 90 min) (Fig. 1A). Dynamic images were acquired in list mode and reframed into a dynamic sequence of 24 frames (10 × 120 s, 14 × 300 s). The resulting sinograms were corrected for scatter, decay time, dead time, and randoms and reconstructed using the OSEM-3D algorithm.

PET images were analyzed using PMOD 3.7 (PMOD Technologies, Zurich, Switzerland). First, the reconstructed PET images were coregistered to their respective MR images using rigid body transformation. Volumes of interest (VOIs) were drawn for the whole brain (WB) using the thresholding tool on the MR image. Regional VOIs (prefrontal cortex, anterior cingulate cortex, caudate, putamen, insula, hippocampus, thalamus, pons, midbrain, and cerebellum) were drawn based on a rhesus template overlaid on the MR images and readjusted manually. Time-activity curves (TACs) for all the regions were generated from the dynamic scans to assess for presence and consistency of nonspecific binding across regions and across various time points (Fig. 1A and B). TACs also indicated that equilibrium was generally achieved between 600 and 2,100 s after 18F-DPA714 injection and from 3,000 to 4,800 s after displacement with cold PK11195 (Fig. 1A). The dynamic data were then summed between 600 and 2,100 s, and the resulting static images were used to generate total standardized uptake values (SUV_T) corresponding to total binding. Similarly, data acquired from 3,300 to 4,800 s were summed to generate a static image which was used to calculate SUVs for nonspecific binding of 18F-DPA714. Binding potential (BP_{ND}) values were then determined as (total binding – nonspecific binding)/nonspecific binding (36). Only whole-brain binding values were calculated and used for the statistical analysis. Even though we delineated regional VOIs in our animals, those were not used in the statistical analysis due to the known heterogeneity of distribution of microglial activation in SIV infection, as demonstrated by histology in our animals, and because we wanted to limit the number of comparisons to be statistically tested, in order to control the overall type I error, particularly in view of the small sample size (low power).

Cytokine level measurements in the CSF. Concentrations of multiple cytokines and chemokines (GM-CSF, TNF-β, G-CSF, IFN-γ, IL-2, IL-10, IL-15, sCD40L, IL-17a, IL-1Ra, IL-13, IL-1β, IL-4, IL-5, IL-6, IL-8, MIP-1α, MCP-1, TNF-α, MIP-1β, vascular endothelial growth factor [VEGF], IL-18, and IL-12) were measured in the CSF of the infected animals within a few days of each PET scan and just before necropsy, using a bead-based multiplex assay (EMD Millipore; PRcytomag-40K). These were chosen based on literature support for cytokine abnormalities in the setting of HIV/SIV infection and the availability of antibodies that are specific to macaques (14–16). The assay was performed according to the manufacturer's instructions. The assay plates were read on the Bio-Plex 200 System (Bio-Rad).

Multiplex fluorescence immunostaining. Brains from SIV-infected macaques ($n = 5$) and controls ($n = 2$) were obtained using a necropsy procedure that included perfusion with saline followed by 10% buffered formalin. The brains were postfixed overnight in 4% paraformaldehyde and then washed three times in normal saline. Next, the brains were cryoprotected in graded 10%, 20%, and 30% sucrose until they sank in each solution. Finally, the brains were embedded and frozen in optimal-cutting-temperature compound (O.C.T.; Tissue-Tek) and then cut into 10-μm-thick coronal serial cryosections. The striatal

sections which included portions of the caudate, putamen, internal capsule, white matter tracts, and corpus callosum were selected for MIF (see Fig. S1 in the supplemental material).

An immunolabeling protocol was applied to identify the various cell populations using 1:100 guinea pig IgG anti-Iba1 (Synaptic Systems, Goettingen, Germany; catalog no. 234004), 1 μg/ml mouse IgG2a anti-S100 (Millipore Sigma; catalog no. MAB079-1), 1 μg/ml mouse IgG1 anti-NeuN (Millipore Sigma; catalog no. MAB377), and 1:100 rabbit anti-CC3/PARP cocktail (Cell Signaling Technology; catalog no. 9661S and 5625S). The primary immunoreactions were visualized using spectrally compatible Alexa Fluor dye-conjugated secondary antibodies (Thermo Fisher Scientific or Jackson ImmunoResearch). The cell nuclei were counterstained using 1 μg/ml DAPI. All fluorescence signals were imaged using an Axio Imager.Z2 upright scanning wide-field fluorescence microscope (Zeiss) equipped with an Orca Flash 4.0 high-resolution scientific complementary metal oxide semiconductor (sCMOS) camera (Hamamatsu), a 200-W X-cite 200DC broadband light source (Lumen Dynamics), and standard DAPI and appropriate Alexa Fluor filter sets (Semrock). Finally, the image data sets were processed for stitching and illumination correction and imported into Adobe Photoshop CS6 to produce pseudocolored composites.

Due to inherent differences in astrocyte distributions within the stained striatal sections, only qualitative assessment of S100 staining was performed. Quantification of Iba1, NeuN, and CC3/PARP immunofluorescence staining was performed using the FIJI image processing package, based on ImageJ (NIH, Bethesda, MD).

Two rectangular regions of interest (ROIs) were selected in the white matter so as to be of the same size and location between all the animals. Those two ROIs included variable numbers of microglial nodules depending on the animal. Another inclusive ROI was selected around the striatum and white matter (including portions of the corpus callosum) and referred to as the "whole" ROI. Since the size of the whole ROI was slightly different across animals, all the values were normalized to the whole-ROI area. The values from the two control brains were averaged for comparison.

For analyses, we converted the RGB bitmap images to 8-bit grayscale and adjusted the threshold to include only cells of interest and eliminate the background. We then calculated the fluorescence intensity and/or cell density (NeuN) within the ROIs. All images were processed using the same analysis parameters.

Detection of SIV RNA expression using RNAscope assay. The RNAscope assay was performed on formalin-fixed, paraffin-embedded brain sections using the RNAscope 2.5 HD reagent kit-Brown (Advanced Cell Diagnostics, Hayward, CA). Briefly, tissue sections were heated at 60°C for 1 h, deparaffinized in xylene washes, washed in 50% xylene-50% ethanol, and then washed twice in 100% ethanol. Tissues were slowly rehydrated with a series of ethanol and double-distilled water (ddH_2O) washes, added to boiling Target Retrieval solution for 30 min at 98°C, washed in buffer, and treated with hydrogen peroxide reagent for 20 min. The slides were then hybridized with RNAscope probe-V-SIVmac239-vif-env-nef-tar overnight at 40°C. After hybridizations, slides were subjected to signal amplification using the HD 2.5 detection kit, and hybridization signal was detected using a mixture of 3,3′-diaminobenzidine (DAB) solutions A and B (1:60). Slides were counterstained with CAT hematoxylin and visualized and photographed with a Zeiss Axio Imager Z1 microscope (Zeiss).

Statistical analysis. The statistical software programs SAS version 9.4 (SAS Institute Inc., Cary, NC) and Prism (GraphPad, version 7.01) were used for analysis.

To assess whether clinically relevant measurements ($CD4^+$ T-cell counts, CSF/plasma VL, duration of infection, and CSF levels of MCP-1, IL-1ra, IL-2, IL-8, IL-10, IL-15, and IL-18) are predictive of 18F-DPA714 uptake, each measurement was first included individually in a statistical model as an explanatory variable, with SUV_T or BP_{ND} as the response variable. The measurements were then included together in one model to evaluate their combined relationship with SUV_T or BP_{ND}. Because of the repeated-measures nature of the data, a mixed model was fitted to the data. For each model, several variance-covariance matrix structures were considered, and the one with the lowest Bayesian information criterion (BIC) was applied. Model-fit diagnostics were examined to check whether model assumptions were met. Because this is an exploratory study with a relatively small sample size, no multiple-comparisons adjustment was used, i.e., all reported *P* values are unadjusted.

Data availability. The data sets supporting the conclusions of this article are in the supplemental material.

SUPPLEMENTAL MATERIAL

Supplemental material for this article may be found at https://doi.org/10.1128/mBio.00970-19.

FIG S1, TIF file, 1.5 MB.

FIG S2, TIF file, 2.3 MB.

FIG S3, TIF file, 2 MB.

TABLE S1, DOCX file, 0.02 MB.

ACKNOWLEDGMENTS

We thank the veterinary and animal care staff of the NIAID for maintaining the nonhuman primates used in this study, the PET department at the Clinical Center for meticulously performing the scans, Merck for providing raltegravir, and Gilead for providing tenofovir and emtricitabine.

Funding for this study was provided in part by the Intramural Research Program of the National Institute of Allergy and Infectious Diseases (NIAID), National Institutes of Health (NIH), and by the Center for Infectious Diseases, Clinical Center, NIH. This project has also been funded in part with federal funds from the National Cancer Institute, NIH, under contract no. HHSN261200800001E. The content of this publication does not necessarily reflect the views or policies of the Department of Health and Human Services, nor does mentioning of trade names, commercial products, or organizations imply endorsement by the U.S. Government.

The authors have no competing interests that could be perceived as being a conflict of interest.

D. A. Hammoud, K. Matsuda, V. Hirsch, A. Nath, and M. Di Mascio conceived of and designed the study. D. A. Hammoud, S. Sinharay, S. Shah, W. Schreiber-Stainthorp, S. Muthusamy, D. E. Lee, W. C. Reid, K. Matsuda, and M. Di Mascio evaluated the animals and/or collected the data. D. A. Hammoud, S. Sinharay, S. Shah, W. Schreiber-Stainthorp, S. Muthusamy, D. E. Lee, K. Matsuda, C. A. Lee, and D. Maric performed data analysis. F. Basuli performed the radiotracer synthesis and drafted the corresponding parts of Materials and Methods and Results. D. A. Hammoud and P. Wakim performed the statistical analysis. All authors participated in drafting the article and/or revising it critically for intellectual content. All authors gave final approval of the submitted manuscript.

REFERENCES

1. Hagberg L, Cinque P, Gisslen M, Brew BJ, Spudich S, Bestetti A, Price RW, Fuchs D. 2010. Cerebrospinal fluid neopterin: an informative biomarker of central nervous system immune activation in HIV-1 infection. AIDS Res Ther 7:15. https://doi.org/10.1186/1742-6405-7-15.
2. Spudich SS. 2014. CROI 2014: neurologic complications of HIV infection. Top Antivir Med 22:594–601.
3. Spudich SS, Ances BM. 2012. Neurologic complications of HIV infection. Top Antivir Med 20:41–47.
4. Valcour V, Chalermchai T, Sailasuta N, Marovich M, Lerdlum S, Suttichom D, Suwanwela NC, Jagodzinski L, Michael N, Spudich S, van Griensven F, de Souza M, Kim J, Ananworanich J. 2012. Central nervous system viral invasion and inflammation during acute HIV infection. J Infect Dis 206:275–282. https://doi.org/10.1093/infdis/jis326.
5. Guha D, Nagilla P, Redinger C, Srinivasan A, Schatten GP, Ayyavoo V. 2012. Neuronal apoptosis by HIV-1 Vpr: contribution of proinflammatory molecular networks from infected target cells. J Neuroinflammation 9:138. https://doi.org/10.1186/1742-2094-9-138.
6. Scarf AM, Kassiou M. 2011. The translocator protein. J Nucl Med 52:677–680. https://doi.org/10.2967/jnumed.110.086629.
7. Ananworanich J, Sacdalan CP, Pinyakorn S, Chomont N, de Souza M, Luekasemsuk T, Schuetz A, Krebs SJ, Dewar R, Jagodzinski L, Ubolyam S, Trichavaroj R, Tovanabutra S, Spudich S, Valcour V, Sereti I, Michael N, Robb M, Phanuphak P, Kim JH, Phanuphak N. 2016. Virological and immunological characteristics of HIV-infected individuals at the earliest stage of infection. J Virus Erad 2:43–48.
8. James ML, Fulton RR, Vercoullie J, Henderson DJ, Garreau L, Chalon S, Dolle F, Costa B, Selleri S, Guilloteau D, Kassiou M. 2008. DPA-714, a new translocator protein-specific ligand: synthesis, radiofluorination, and pharmacologic characterization. J Nucl Med 49:814–822. https://doi.org/10.2967/jnumed.107.046151.
9. Martin A, Boisgard R, Theze B, Van Camp N, Kuhnast B, Damont A, Kassiou M, Dolle F, Tavitian B. 2010. Evaluation of the PBR/TSPO radioligand [(18)F]DPA-714 in a rat model of focal cerebral ischemia. J Cereb Blood Flow Metab 30:230–241. https://doi.org/10.1038/jcbfm.2009.205.
10. Martin A, Boisgard R, Kassiou M, Dolle F, Tavitian B. 2011. Reduced PBR/TSPO expression after minocycline treatment in a rat model of focal cerebral ischemia: a PET study using [(18)F]DPA-714. Mol Imaging Biol 13:10–15. https://doi.org/10.1007/s11307-010-0324-y.
11. Matsuda K, Dang Q, Brown CR, Keele BF, Wu F, Ourmanov I, Goeken R, Whitted S, Riddick NE, Buckler-White A, Hirsch VM. 2014. Characterization of simian immunodeficiency virus (SIV) that induces SIV encephalitis in rhesus macaques with high frequency: role of TRIM5 and major histocompatibility complex genotypes and early entry to the brain. J Virol 88:13201–13211. https://doi.org/10.1128/JVI.01996-14.
12. Imai Y, Kohsaka S. 2002. Intracellular signaling in M-CSF-induced microglia activation: role of Iba1. Glia 40:164–174. https://doi.org/10.1002/glia.10149.
13. Chaitanya GV, Steven AJ, Babu PP. 2010. PARP-1 cleavage fragments: signatures of cell-death proteases in neurodegeneration. Cell Commun Signal 8:31. https://doi.org/10.1186/1478-811X-8-31.
14. Hong S, Banks WA. 2015. Role of the immune system in HIV-associated neuroinflammation and neurocognitive implications. Brain Behav Immun 45:1–12. https://doi.org/10.1016/j.bbi.2014.10.008.
15. Huang X, Liu X, Meyers K, Liu L, Su B, Wang P, Li Z, Li L, Zhang T, Li N, Chen H, Li H, Wu H. 2016. Cytokine cascade and networks among MSM HIV seroconverters: implications for early immunotherapy. Sci Rep 6:36234. https://doi.org/10.1038/srep36234.
16. Ramesh G, Philipp MT, Vallieres L, MacLean AG, Ahmad M. 2013. Mediators of neuroinflammation. Mediators Inflamm 2013:314261. https://doi.org/10.1155/2013/314261.
17. Selya AS, Rose JS, Dierker LC, Hedeker D, Mermelstein RJ. 2012. A practical guide to calculating Cohen's f(2), a measure of local effect size, from PROC MIXED. Front Psychol 3:111. https://doi.org/10.3389/fpsyg.2012.00111.
18. Cosenza MA, Zhao ML, Si Q, Lee SC. 2002. Human brain parenchymal microglia express CD14 and CD45 and are productively infected by HIV-1 in HIV-1 encephalitis. Brain Pathol 12:442–455.
19. Avalos CR, Price SL, Forsyth ER, Pin JN, Shirk EN, Bullock BT, Queen SE, Li M, Gellerup D, O'Connor SL, Zink MC, Mankowski JL, Gama L, Clements JE. 2016. Quantitation of productively infected monocytes and macrophages of simian immunodeficiency virus-infected macaques. J Virol 90:5643–5656. https://doi.org/10.1128/JVI.00290-16.
20. Cenker JJ, Stultz RD, McDonald D. 2017. Brain microglial cells are highly susceptible to HIV-1 infection and spread. AIDS Res Hum Retroviruses 33:1155–1165. https://doi.org/10.1089/AID.2017.0004.
21. Castellano P, Prevedel L, Eugenin EA. 2017. HIV-infected macrophages and microglia that survive acute infection become viral reservoirs by a mechanism involving Bim. Sci Rep 7:12866. https://doi.org/10.1038/s41598-017-12758-w.
22. Kramer-Hammerle S, Rothenaigner I, Wolff H, Bell JE, Brack-Werner R. 2005. Cells of the central nervous system as targets and reservoirs of the human immunodeficiency virus. Virus Res 111:194–213. https://doi.org/10.1016/j.virusres.2005.04.009.
23. Chen NC, Partridge AT, Tuzer F, Cohen J, Nacarelli T, Navas-Martin S, Sell C, Torres C, Martin-Garcia J. 2018. Induction of a senescence-like phe-

notype in cultured human fetal microglia during HIV-1 infection. J Gerontol A Biol Sci Med Sci 73:1187–1196. https://doi.org/10.1093/gerona/gly022.
24. Matsuda K, Brown CR, Foley B, Goeken R, Whitted S, Dang Q, Wu F, Plishka R, Buckler-White A, Hirsch VM. 2013. Laser capture microdissection assessment of virus compartmentalization in the central nervous systems of macaques infected with neurovirulent simian immunodeficiency virus. J Virol 87:8896–8908. https://doi.org/10.1128/JVI.00874-13.
25. Matsuda K, Riddick NE, Lee CA, Puryear SB, Wu F, Lafont BAP, Whitted S, Hirsch VM. 2017. A SIV molecular clone that targets the CNS and induces neuroAIDS in rhesus macaques. PLoS Pathog 13:e1006538. https://doi.org/10.1371/journal.ppat.1006538.
26. Doorduin J, Klein HC, Dierckx RA, James M, Kassiou M, de Vries EF. 2009. [11C]-DPA-713 and [18F]-DPA-714 as new PET tracers for TSPO: a comparison with [11C]-(R)-PK11195 in a rat model of herpes encephalitis. Mol Imaging Biol 11:386–398. https://doi.org/10.1007/s11307-009-0211-6.
27. Chauveau F, Van Camp N, Dolle F, Kuhnast B, Hinnen F, Damont A, Boutin H, James M, Kassiou M, Tavitian B. 2009. Comparative evaluation of the translocator protein radioligands 11C-DPA-713, 18F-DPA-714, and 11C-PK11195 in a rat model of acute neuroinflammation. J Nucl Med 50:468–476. https://doi.org/10.2967/jnumed.108.058669.
28. Coughlin JM, Wang Y, Ma S, Yue C, Kim PK, Adams AV, Roosa HV, Gage KL, Stathis M, Rais R, Rojas C, McGlothan JL, Watkins CC, Sacktor N, Guilarte TR, Zhou Y, Sawa A, Slusher BS, Caffo B, Kassiou M, Endres CJ, Pomper MG. 2014. Regional brain distribution of translocator protein using [(11)C]DPA-713 PET in individuals infected with HIV. J Neurovirol 20:219–232. https://doi.org/10.1007/s13365-014-0239-5.
29. Vera JH, Guo Q, Cole JH, Boasso A, Greathead L, Kelleher P, Rabiner EA, Kalk N, Bishop C, Gunn RN, Matthews PM, Winston A. 2016. Neuroinflammation in treated HIV-positive individuals: a TSPO PET study. Neurology 86:1425–1432. https://doi.org/10.1212/WNL.0000000000002485.
30. Carson RE. 2000. PET physiological measurements using constant infusion. Nucl Med Biol 27:657–660. https://doi.org/10.1016/S0969-8051(00)00138-4.
31. Wu F, Kirmaier A, Goeken R, Ourmanov I, Hall L, Morgan JS, Matsuda K, Buckler-White A, Tomioka K, Plishka R, Whitted S, Johnson W, Hirsch VM. 2013. TRIM5 alpha drives SIVsmm evolution in rhesus macaques. PLoS Pathog 9:e1003577. https://doi.org/10.1371/journal.ppat.1003577.
32. Wu F, Ourmanov I, Riddick N, Matsuda K, Whitted S, Plishka RJ, Buckler-White A, Starost MF, Hirsch VM. 2015. TRIM5alpha restriction affects clinical outcome and disease progression in simian immunodeficiency virus-infected rhesus macaques. J Virol 89:2233–2240. https://doi.org/10.1128/JVI.02978-14.
33. Hines CS, Fujita M, Zoghbi SS, Kim JS, Quezado Z, Herscovitch P, Miao N, Ferraris Araneta MD, Morse C, Pike VW, Labovsky J, Innis RB. 2013. Propofol decreases in vivo binding of 11C-PBR28 to translocator protein (18 kDa) in the human brain. J Nucl Med 54:64–69. https://doi.org/10.2967/jnumed.112.106872.
34. Saba W, Goutal S, Kuhnast B, Dolle F, Auvity S, Fontyn Y, Cayla J, Peyronneau MA, Valette H, Tournier N. 2015. Differential influence of propofol and isoflurane anesthesia in a non-human primate on the brain kinetics and binding of [(18)F]DPA-714, a positron emission tomography imaging marker of glial activation. Eur J Neurosci 42:1738–1745. https://doi.org/10.1111/ejn.12946.
35. Kuhnast B, Damont A, Hinnen F, Catarina T, Demphel S, Le Helleix S, Coulon C, Goutal S, Gervais P, Dollé F. 2012. [18F]DPA-714, [18F]PBR111 and [18F]FEDAA1106-selective radioligands for imaging TSPO 18 kDa with PET: automated radiosynthesis on a TRACERLAb FX-FN synthesizer and quality controls. Appl Radiat Isot 70:489–497. https://doi.org/10.1016/j.apradiso.2011.10.015.
36. Nabulsi N, Huang Y, Weinzimmer D, Ropchan J, Frost JJ, McCarthy T, Carson RE, Ding YS. 2010. High-resolution imaging of brain 5-HT 1B receptors in the rhesus monkey using [11C]P943. Nucl Med Biol 37:205–214. https://doi.org/10.1016/j.nucmedbio.2009.10.007.